Lasers in Manufacturing Conference 2023

Hybrid approaches for reducing defects in laser-based direct energy deposition of nickel-based superalloys

M. Müller[a,b,*], S. Poetke[b], M. Heckert[a], M. Riede[b], E. López[b], F. Brueckner[b,c], C. Leyens[a,b]

[a]*Technische Universität Dresden, Insitute of Material Science, Helmholtzstr. 7, 01069 Dresden, Germany*
[b]*Fraunhofer IWS, Winterbergstraße 28, Dresden, Germany*
[c]*Luleå University of Technology, 971 87 Luleå, Sweden*

Abstract

Due to their outstanding high temperature properties, nickel-based superalloys are among the key materials in the energy and aerospace sector. With increasing importance of the additive manufacturing technology, direct energy deposition (DED) for industrial applications, such as the repair of turbine blades, DED of nickel-based superalloys has become a research field of high relevance.
However, the formation of defects in fabricated components (e.g. solidification cracking) is impeding the industrial transfer. Within this contribution the combination of DED with additional physical effects (hybrid DED) such as inductive heating or static and dynamic magnetic fields and their impact on crack mitigation is presented. The described approaches were examined based on studies on DED of crack-prone alloys such as Mar-M-247 and Ni-SA 247 LC. The results show the potential but also the limitations of hybrid DED depending on material and process specific challenges.

Keywords: additive manufacturing; direct energy deposition; nickel-based superalloys; hybrid manufacturing; crack mitigation

1. Introduction

Within the last years, laser-based direct energy deposition (L-DED) with blown powder has emerged as one of the major techniques for additive manufacturing (AM) as well as maintenance and repair (MRO) [1,2]. In L-DED with blown powder, an inert gas stream conveys a powdery feedstock material into the process zone, where it is preheated by a laser beam and finally absorbed by the laser-induced melt pool [2]. The nozzle based deposition systems are mostly integrated into customized CNC machines or robot systems. In contrast to other AM technologies, such as laser powder bed fusion (PBF-LB), this technology can be not only used for bare AM but also to modify or repair already existing components in a hybrid manner [3,4]. Due to the high

flexibility of the process with respect to its thermal boundary conditions, especially the processing of hardly or even non-weldable materials has evolved as a major research field in L-DED. Within this class of advanced materials, nickel-based superalloys have been widely investigated [5-9]. Due to their outstanding high temperature properties, nickel-based superalloys are among the major materials in the aerospace and energy sector and are commonly used in modern gas turbines or jet engines. Hence, AM and MRO using nickel-based superalloys can contribute significantly to an increased sustainability within these branches [10,11].

However, commonly used high performance nickel-based superalloy, e.g. Mar-M-247, CMSX-4 or IN 100, are considered as non-weldable due to their susceptibility to hot cracking [12]. Hot cracking is referred to as interdendritic cracking occurring when the material is passing the interval between solidus and liquids temperature. In dependence whether the cracking occurs within the remelted base material or the solidifying filler material, liquation and solidification cracking are distinguished. The main phenomenon causing the formation of hot cracks are microsegregations due to varying partition coefficients of different elements contained by the named alloys. Elements exhibiting a partition coefficient $k > 1$ (e.g. $k_{Al} = 0.86; k_{Ti} = 0.86$ for CMSX-4 according to [13]) tend to diffuse into the interdendritic regions during solidification causing a local drop in liquidus temperatures. This leads to undercooled liquid films within the interdendritic areas. Due to strain caused by the shrinkage during solidification, these films tend to be torn apart and initiate interdendritic cracking [12,14]. Since numerous parts in gas turbines and jet engines are exposed to static as well as dynamic loads, these cracks can have detrimental effects on the components' lifetime and therefore need to be eliminated. In order to overcome this challenge, the solidification conditions need to be controlled precisely during the deposition process [12,13-15].

A promising approach for overcoming this challenge is hybrid manufacturing, which combines L-DED with further energy sources, such as induction heating of the substrate or electromagnet forces [14-21].

On one hand, a reduction of thermally induced stresses by lowering thermal gradients can be achieved by an inductive high temperature preheating of the substrate. Bidron et al. [14] as well as Seidel et al. [15] and McNut [16] performed studies on induction assisted L-DED of the alloy CM 247 LC and showed the beneficial influence of this approach on the reduction of hot cracking. Additionally, Rottwinkel et al. [17] applied this approach for the mitigation of cracks in L-DED of CMSX-4.

On the other hand, magneto-fluid dynamic mechanisms can be applied for modifying the flow characteristics within the melt pool [18-22]. Due to the interaction between the electromagnetic fields and the molten metal characteristic phenomena such as the Hartmann flow and the Ekman jet can be induced leading to a change in velocity amplitude and distribution within the melt pool. Most studies observed that static as well as rotating electromagnetic fields induce a grain refinement in the solidified material [18-20]. In addition, Seidel et al. [22] also observed a beneficial impact of the applied electromagnetic fields on the reduction of hot cracks caused by the modification of the melt pool convection.

Within this contribution, we discuss previous work jointly performed by Technische Universität Dresden and Fraunhofer IWS [15, 22-24] and present recent advances in processing the nickel-based superalloys Mar-M-247, CM 247 LC and Ni-SA 247 LC by combining L-DED with inductive heating and electromagnetic stirring.

2. Materials and Methods

2.1. Materials

Within the presented studies the nickel-based superalloy Mar-M-247 or the adapted derivatives of this alloy, namely Ni-SA 247 LC and CM 247 LC were used. The compositions of the used alloys are shown in Table 1. Due to their high fraction in γ' phase (approx. 62 %) these alloys are considered as non-weldable and severely

tend to form solidification and liquation cracks. Ni-SA 247 LC powder (d_{10} = 15 µm and d_{90} = 45 µm) as well as substrate material were used for the presented experiments on electromagnetic stirring. The baseline induction heating trials were performed using Mar-M-247 powder material (d_{10} = 51 µm and d_{90} = 94 µm) and various substrate materials such as Mar-M-247, Inconel 625 as well as Inconel 718 substrate material. The following induction assisted manufacturing of the presented blade tip was conducted using CM 247 LC powder material (d_{10} = 27 µm and d_{90} = 51 µm) and Inconel 718 substrates.

Table 1. Overview of the chemical composition of the materials used in the presented studies

Alloy	**Chemical composition in wt.-%**									
	Al	**Ti**	Cr	Co	Mo	W	Hf	Ta	C	**Ni**
Ni-SA 247LC	5.6	0.8	8.2	9.2	0.5	9.3	1.4	3.2	0.06	**balance**
Mar-M-247	5.5	1.0	8.25	10.0	0.7	10.0	1.5	3.0	0.15	**balance**
CM 247 LC	5.6	0.7	8.1	9.2	0.5	9.5	1.4	3.2	0.07	**balance**

2.2. Inductive preheating

In order to achieve an efficient inductive preheating and a homogeneous temperature distribution the frequency of the applied electromagnet fields needs to be adapted to the part geometry. For the preheating of the round bars (d = 25 mm) shown in Figure 1 middle frequency induction generators with a frequency between 10 kHz and 25 kHz were used.

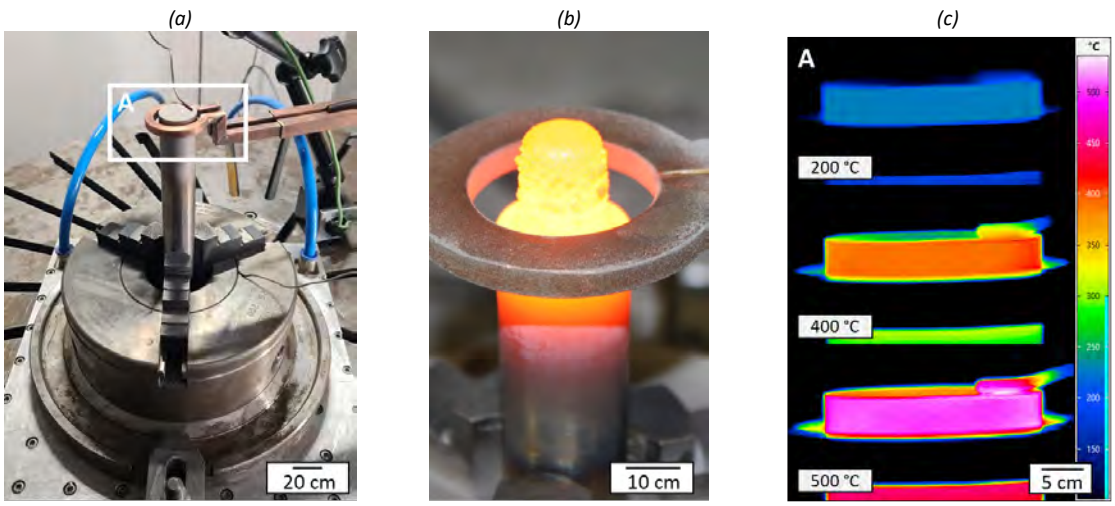

Fig. 1. (a) Exemplary process set up for the preheating of cylindircal substrate and cylindrial specimens, (b) preheated substrate and sample during manufacturing, (c) infrared image of a substrate during preheating before deposition as shown in (a)

The used coil exhibits a ring-like geometry assuring a homogenous heating of the substrate. The deposition took place using a COAXpowerline powder nozzle (Fraunhofer IWS, Germany) for processing without preheating and a COAX 14 nozzle (Fraunhofer IWS, Germany) for depositions with inductive preheating.

Figure 1a and b show an exemplary process set up using a round substrate and ring shape induction coil. In order to obtain a precise preheating temperature measurement by means of radiation thermometry is applied (Figure 1c). The specimens presented in section 3.1 were deposited with the following parameters on various substrates such as Inconel 625, Inconel 718 or Mar-M-247.

Table 2. Overview of process parameters used for the fabrication of the different Mar-M-247 samples shown in this work

Sample	Substrate temperature in °C	Laser power in Watt	Deposition speed in mm/min	Powder mass rate in g/min
RT sample	room temperature	450	500	**1**
HT sample	900 °C	550	500	**1.7**
Blade sample	1100 °C	550	500	**1.7**

2.3. Electromagnetic stirring

In order to investigate the influence of temporarily constant and rotating magnetic fields on the solidification process during L-DED, a magnet rotation device was developed (Figure 2). The main component of this device is a customized electromagnet. This can be used to generate a constant and homogeneous magnetic field in a centric air gap of 10 mm width with a magnetic flux density of up to 1 T.

The magnet is integrated into a device that enables a rotational movement of the magnet up to 20 Hz as well as a relative rotational movement of a substrate in the center of the air gap for the welding process. Via the substrate rotation, a feed during the welding process can be realized without the need for a translational movement of the process head. As a result, the molten pool position is constant in relation to the external magnetic field during the process.

Fig. 2. Experimental set up for the investigation of the influence of static and rotating electromagnetic fields on the solidifcation microstructure and crack formation

L-DED was carried out using a COAX 16 powder nozzle (Fraunhofer IWS, Germany) in combination with a 1 kW Rofin FL010C fiber laser (Coherent Inc., United States). A disc powder feeding system from GTV Verschleißschutz GmbH (Germany) was used to convey the powder material.

Prior to manufacturing, the magnetic field was characterized using a KOSHAVA 5 gaussmeter (Wuntronic, Germany). The results, presented in Figure 3, show that the targeted magnetic flux density of 1 T can be reached at a power of approx. 800 W. Moreover, the results show that with increasing vertical distance from the initial position a drop of approx. 15 % occurs until a height of 10 mm.

The specimens presented in this work were manufactured using a laser power of 300 W, a welding speed of 500 mm/min and a powder mass rate of 2 g/min. All samples presented were fabricated with identical parameters. The specimens consist of three circular tracks with a track height of approx. 0.2 mm, a track width of approx. 1 mm and an overlap of 50 %. Two layers were applied on top of each other forming a hollow cylinder structure. Centric cross sections were investigated by light optical microscopy, scanning electron microscopy (SEM), energy dispersive X-ray spectroscopy (EDS) and electron backscatter diffraction (EBSD).

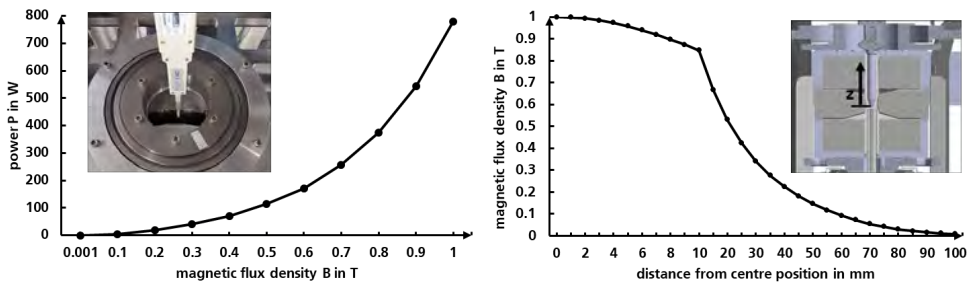

Fig. 3. Characterization of the electromagnetic properties of the experimental set up showing maximum magnetic flux densities of up to 1 T (left) and the spatial deviations of the magnetic flux density in z-direction (right)

3. Results and Discussion

3.1. Inductive preheating

As described in section 2 middle frequency induction generators were used to achieve a high temperature preheating of up to 1100 °C. In Figure 4 two specimens made of Mar-M-247, one fabricated without substrate preheating (Figure 4a) and the other with a preheating temperature of 900 °C (Figure 4b), are compared. As can be seen in Table 2 similar process parameters were used for the fabrication.

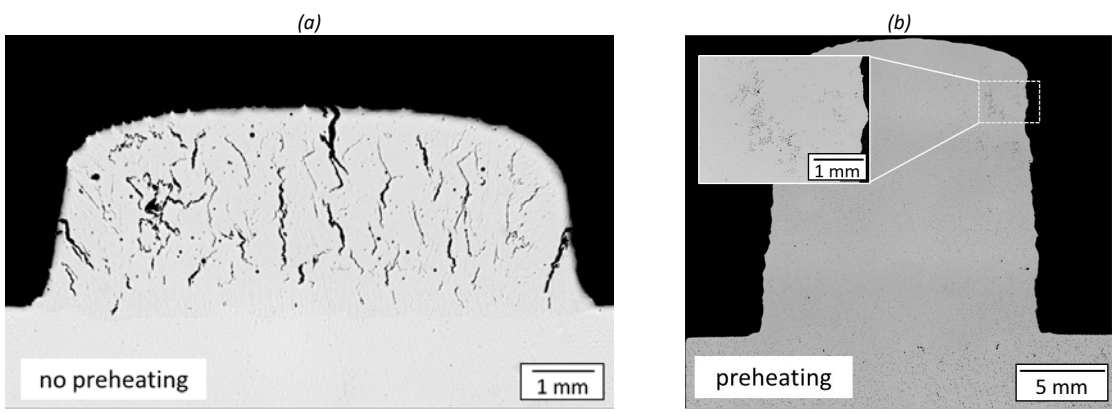

Fig. 4. Deposited Mar-M-247 on Inconel 625 substrate material deposited without preheating (a) and Mar-M-247 deposited on Mar-M-247 with a preheating temperature of 900 °C (b)

Hence, it is evident that by applying the high temperature preheating a significant reduction of hot cracking can be achieved. However, as can be seen in Figure 4b a small degree of interdendritic cavities is still present in this specimen. The reduction of cracking is attributed to the decrease in thermally induced stresses as well as the reduction of cooling rates.

Based on these promising results, Maiwald [23] transferred the process to the near net shape manufacturing of a CM 247 LC blade tip with tailored inductive preheating. The results show how inductive preheating can be applied also to non-symmetrical parts with the goal of an increased complexity of the deposited structure. Figure 5 presents the manufactured blade tip (Figure 5a) and two cross sections in etched condition (Figure 5b and c). For the fabrication of this structure, a preheating temperature of 1100 °C and the parameters shown in Table 2 were applied.

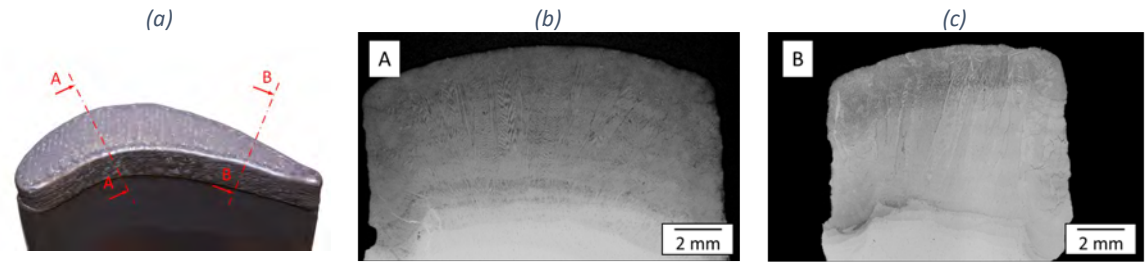

Fig. 5. (a) Deposited CM 247 LC on Inconel 718 substrate material as a near net shape blade geometry. The substrate was preheated to 1100 °C to obtain a reduction of defects, (b) etched cross section at position A, (c) etched cross section at position B, all images adapted from [23]

Fig. 6. (a) Mar-M-247 blade demonstrator manufactured with inductive preheating. The specimen on the left was manufactured with non-controlled process whereas and the specimen on the right with a closed-loop control of the working distance; adapted from [24]; (b) monitoring image of the hybrid manufacturing using induction heating taken from [25]

However, due to the need of a near net shape induction coil to achieve an efficient preheating, processing of complex parts can pose severe challenges with respect to achieving a homogeneous temperature distribution. Especially with increasing build height and a fixed position of the induction coil a decrease in preheating temperature takes place. In order to overcome this, Willner [24] developed a procedure for an in-situ adaption of the induction power with increasing build height and varying part geometry. In addition to this, a system for measuring and controlling the working distance between nozzle and substrate was applied. By combining these tools, the blade specimen shown in Figure 6a was fabricated. Figure 6b shows an exemplary image of the developed system for temperature monitoring and working distance control.

The results show the great benefit of induction heating of the substrate for overcoming hot cracking related challenges. Moreover, the results by Willner [24] show that additional tools, such as working distance control, are mandatory for achieving a stable hybrid manufacturing process. In addition to the processing of Mar-M-247, Brueckner et al. [25] adapted this approach for the fabrication of parts made of titanium aluminides and showed how hybrid manufacturing can be used to increase the number of available materials in AM.

3.2. Electromagnetic stirring

Using the system described in section 2.3, samples were manufactured and thoroughly analyzed. Light optical microscopy images of cross sections, shown in Figure 7, reveal that for samples fabricated with and without an external electromagnetic field, hot cracking within the samples can be observed. Both samples show vertical cracking initiated in the partially melted zone between the first layer and the substrate. Additionally, liquation cracking initiated within the first layer and then propagating into the top layer can be identified. Regarding the origin of cracking as well the length and distribution of cracks, no major influence of the external electromagnetic field can be derived.

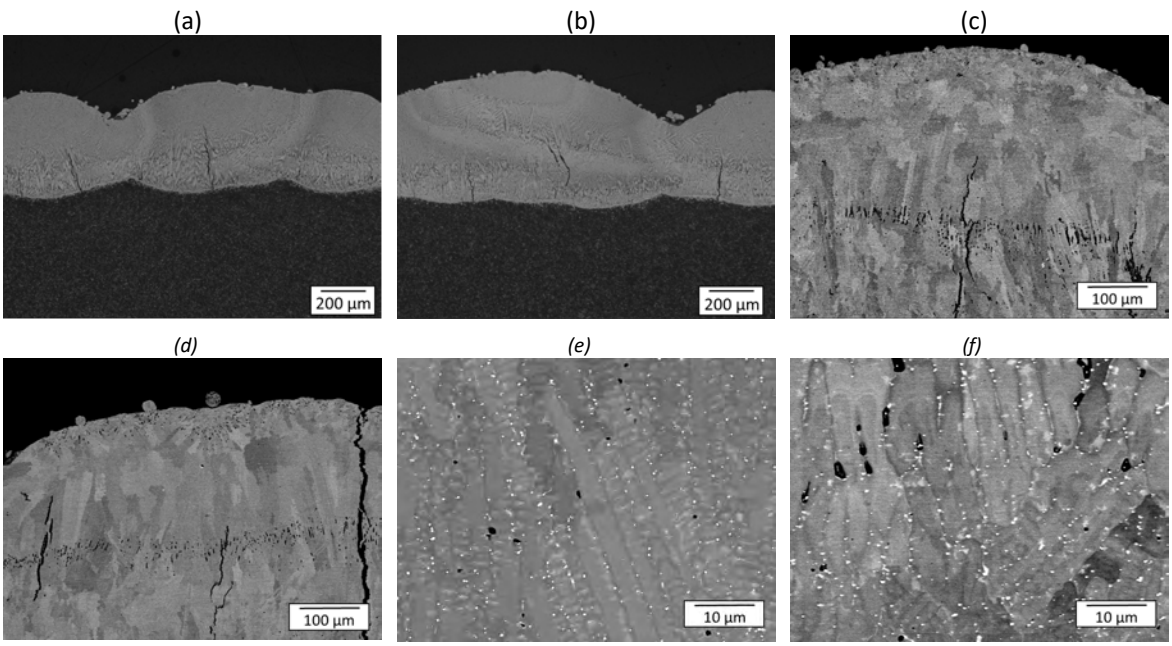

Fig. 7. (a-b) Optical microscopy images of centric cross sections of Ni-SA 247LC fabricated without (a) and with (b) an external electromagnetic field (B = 1 T, f = 12 Hz); (c-f) SEM images of centric cross sections of Mar-M-247 fabricated without (c, e) and with (d, f) an external electromagnetic field (B = 1 T, f = 12 Hz)

Furthermore, SEM of the sample cross sections was performed. The SEM images are presented in Figure 7. The overview images of the top regions (Figure 7c and d) show the formation of small and evenly distributed defects at the interface between the first and the second layer. Additionally, the propagation of cracks from the first into the second layer is evident. The morphology of the cracks suggests an intercrystalline propagation. Close to the surface of the second layer, small defects are present in both samples. The sample processed with electromagnetic stirring even shows a higher degree of defect formation in comparison to the conventionally fabricated specimen. Both samples exhibit a transition from a columnar to an equiaxed dendritic structure. SEM images at higher magnifications (Figure 7e, f) show the presence of a dendritic microstructure in both samples. Additionally, a large number of carbides primarily located at the grain boundaries can be observed. EDS measurements showed that the carbides are rich in refractory elements such as Ta and Hf. Regarding the carbide formation also no difference due to the external electromagnetic field could be observed.

EBSD analysis of the grain structure revealed a strong alignment of the crystallographic [001] direction with the specimen x-axis (built-up direction). This can be seen in the inverse pole figures presented in Figure 8a and b. Comparing the two specimens shows that the sample processed with an applied external electromagnetic field shows an even stronger tendency to the [001] direction. This observation is contrary to the expectations as the electromagnetically induced stirring was expected to enhance the grain refinement and homogenize the crystal structure as was observed by Lui et al. [19] as well as Shi et al. [20]. Also, a lack of grain refinements was identified as both samples show similar grain sizes.

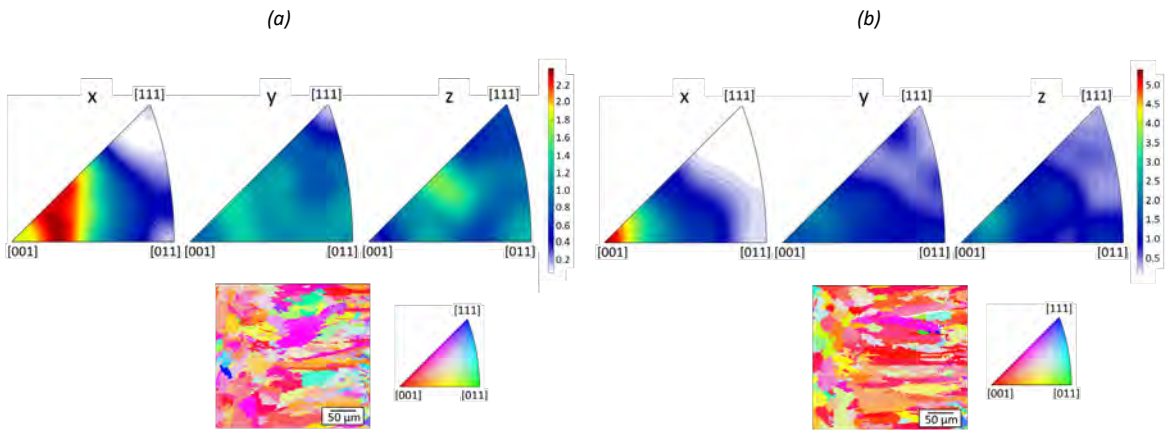

Fig. 8. EBSD inverse pole figures and orientation mapping (x-direction) of Mar-M-247 fabricated without (a) and with (b) external electromagnetic field (B = 1 T, f = 12 Hz). x corresponds to the sample width (transverse direction), y to the sample height (rolling direction) and z to the out-of-plane direction (sample normal).

The main reasons for the absence of any detectable influence of the applied electromagnetic field on the microstructures are one hand the small melt pool dimensions used in this work (1 mm width and 0.2 mm height). Based on equation 1 and data from previous work by Seidel et al. [22] a Hartmann number of approx. 10 can be estimated for a magnetic flux density of 1 T and a melt pool width of 1 mm. However, this value can

be expected as the lower limit for a significant influence of the electromagnetic field on the melt pool. Since the Hartmann number is proportional to the melt pool width L, an increase in melt pool dimensions could significantly improve the interaction and should be considered in further investigations.

$$Ha = B \cdot L \cdot \sqrt{\frac{\sigma}{\eta}} \qquad (1)$$

On the other hand, with small melt pool dimensions and a rather high deposition speed (500 mm/min), high cooling rates and short interaction durations between the electromagnetic field and the melt pool can be expected. This might also contribute to a lack of microstructure modification.

4. Summary and Conclusion

The presented work shows how hybrid approaches, such as inductive heating and electromagnetic stirring can help to overcome hot cracking related challenges. However, the results also show limitations regarding process boundary conditions, such as melt pool size and welding speed that have to be considered for process development. All in all the following major findings were made and conclusions drawn:

- Inductive preheating of the substrate enables a local preheating to over 1000 °C and can significantly contribute to a reduction of hot cracking. For applying this approach to parts with a higher degree of complexity, a monitoring and in-situ adaption of the induction parameters is necessary. This approach is useful to process Ni-based superalloys, such as Mar-M-247, and can be also transferred to other hard-to-weld metals such as TiAl- and NiAl-based alloys.
- A system was developed to perform L-DED in combination with external static and dynamic electromagnetic fields. Experimental characterization of the set up showed that a magnetic flux density of up to 1 T and rotation frequencies of up to 12 Hz can be realized. Multi-layer build-ups could be manufactured successfully using the developed set up.
- Microstructural analysis of the fabricated samples did not show any significant influence of the electromagnetic fields, which is contradicting preliminary trials and findings in literature. The small melt pool dimensions and rather high welding speeds are assumed to be the major reasons for this. Hence, in order to enhance the interaction between melt pool and electromagnetic field a melt pool width significantly larger than 1 mm and welding speeds below 500 mm/min should be used in order to increase the Hartmann and Ekman flow.

Acknowledgements

This work was partially funded by the German Research Foundation (Deutsche Forschungsgemeinschaft (DFG)) under the grant number 396298896.

References

[1] Kaierle, Stefan; Barroi, Alexander; Noelke, Christian; Hermsdorf, Joerg; Overmeyer, Ludger; Haferkamp, Heinz (2012): Review on Laser Deposition Welding: From Micro to Macro. In: *Physics Procedia* 39, S. 336–345. DOI: 10.1016/j.phpro.2012.10.046.

[2] Dass, Adrita; Moridi, Atieh (2019): State of the Art in Directed Energy Deposition: From Additive Manufacturing to Materials Design. In: *Coatings* 9 (7), S. 418. DOI: 10.3390/coatings9070418.

[3] Polenz, Stefan; Kolbe, Christian; Bittner, Florian; López, Elena; Brueckner, Frank; Leyens, Christoph (2021): Integration of pure copper to optimize heat dissipation in injection mould inserts using laser metal deposition. In: *Journal of Laser Applications* 33 (1), S. 12029. DOI: 10.2351/7.0000303.

[4] Saboori, Abdollah; Aversa, Alberta; Marchese, Giulio; Biamino, Sara; Lombardi, Mariangela; Fino, Paolo (2019): Application of Directed Energy Deposition-Based Additive Manufacturing in Repair. In: *Applied Sciences* 9 (16), S. 3316. DOI: 10.3390/app9163316.

[5] Jinoop, Arackal Narayanan; Paul, Christ; Bindra, K. S. (2019): Laser-assisted directed energy deposition of nickel super alloys: A review. In: *Proceedings of the IMechE* 233 (11), S. 2376–2400. DOI: 10.1177/1464420719852658.

[6] Petrat, Torsten; Brunner-Schwer, Christian; Graf, Benjamin; Rethmeier, Michael (2019): Microstructure of Inconel 718 parts with constant mass energy input manufactured with direct energy deposition. In: *Procedia Manufacturing* 36, S. 256–266. DOI: 10.1016/j.promfg.2019.08.033.

[7[Alhuzaim, Abdullah; Imbrogno, Stano; Attallah, Moataz M. (2021): Direct laser deposition of crack-free CM247LC thin walls: Mechanical properties and microstructural effects of heat treatment. In: *Materials & Design* 211, S. 110123. DOI: 10.1016/j.matdes.2021.110123.

[8] Bidare, Prveen; Mehmeti, Aldi; Jiménez, Amaia; Li, Sheng; Garman, Chris; Dimov, Stefan; Essa, Khamis (2022): High-density direct laser deposition (DLD) of CM247LC alloy: microstructure, porosity and cracks. In: *Int J Adv Manuf Technol* 120 (11-12), S. 8063–8074. DOI: 10.1007/s00170-022-09289-8.

[9] Mazzucato, Federico; Forni, Daniele; Valente, Anna; Cadoni, Ezio (2021): Laser Metal Deposition of Inconel 718 Alloy and As-built Mechanical Properties Compared to Casting. In: *Materials (Basel, Switzerland)* 14 (2). DOI: 10.3390/ma14020437.

[10] Bennett, Jennifer; Garcia, Daniel; Kendrick, Marie; Hartman, Travis; Hyatt, Gregory; Ehmann, Kornel et al. (2019): Repairing Automotive Dies With Directed Energy Deposition: Industrial Application and Life Cycle Analysis. In: *Journal of Manufacturing Science and Engineering* 141 (2), Artikel 021019. DOI: 10.1115/1.4042078.

[11] Piscopo, Gabriele; Iuliano, Luca (2022): Current research and industrial application of laser powder directed energy deposition. In: *Int J Adv Manuf Technol* 119 (11-12), S. 6893–6917. DOI: 10.1007/s00170-021-08596-w.

[12] Catchpole-Smith, S.; Aboulkhair, N.; Parry, L.; Tuck, C.; Ashcroft, I. A.; Clare, A. (2017): Fractal scan strategies for selective laser melting of 'unweldable' nickel superalloys. In: *Additive Manufacturing* 15, S. 113–122. DOI: 10.1016/j.addma.2017.02.002.

[13] Bürgel, Ralf; Maier, Hans Jürgen. Niendorf, Thomas (2011): Handbuch Hochtemperatur-Werkstofftechnik. Grundlagen, Werkstoffbeanspruchungen, Hochtemperaturlegierungen und -beschichtungen ; mit 66 Tabellen. 4., überarb. Auflage. Wiesbaden: Vieweg + Teubner (Praxis).

[14] Bidron, Guillaume; Doghri, Anis; Malot, Thierry; Fournier-dit-Chabert, Florent; Thomas, Marc; Peyre, Patrice (2020): Reduction of the hot cracking sensitivity of CM-247LC superalloy processed by laser cladding using induction preheating. In: *Journal of Materials Processing Technology* 277, S. 116461. DOI: 10.1016/j.jmatprotec.2019.116461.

[15] Seidel, André; Finaske, Thomas; Straubel, Ariane; Wendrock, Horst; Maiwald, Tim; Riede, Mirko et al. (2018): Additive Manufacturing of Powdery Ni-Based Superalloys Mar-M-247 and CM 247 LC in Hybrid Laser Metal Deposition. In: *Metall and Mat Trans A* 49 (9), S. 3812–3830. DOI: 10.1007/s11661-018-4777-y.

[16] McNutt, Philip Alexander (2015): An investigation of cracking in laser metal deposited nickel superalloy CM247LC. University of Birmingham.

[17] Rottwinkel, Boris; Nölke, Christian; Kaierle, Stefan; Wesling, Volker (2017): Laser Cladding for Crack Repair of CMSX-4 Single-Crystalline Turbine Parts. In: *Lasers Manuf. Mater. Process.* 4 (1), S. 13–23. DOI: 10.1007/s40516-016-0033-8.

[18] Kern, M.; Berger, Peter; Hügel, Helmut (2000): Magneto-Fluid Dynamic Control of Seam Quality in CO2 Laser Beam Welding 79, 72s-78s.

[19] Liu, Fencheng; Cheng, Hongmao; Yu, Xiaobin; Yang, Guang; Huang, Chunping; Lin, Xin; Chen, Jing (2018): Control of microstructure and mechanical properties of laser solid formed Inconel 718 superalloy by electromagnetic stirring. In: *Optics & Laser Technology* 99, S. 342–350. DOI: 10.1016/j.optlastec.2017.09.022.

[20] Shi, Yongjun; Zhou, Xiaoyu; Wang, Xiaogang; Feng, Xingteng; Peng, Laida (2022): Effects of Electromagnetic Fields on the Microstructure of Laser Cladding. In: *Materials (Basel, Switzerland)* 15 (12). DOI: 10.3390/ma15124198.

[21] Zhai, Lu Lu; Zhang, Jun Wei; Ban, Chun Yan (2019): Influence on the Microstructure of Laser Cladding NiCrBSi Coatings with Electromagnetic Compound Field. In: *SSP* 295, S. 15–20. DOI: 10.4028/www.scientific.net/SSP.295.15.

[22] Seidel, André; Degener, Luise; Schneider, Jacob; Brueckner, Frank; Beyer, Eckhard; Leyens, Christoph (2020): Novel Approach for Suppressing of Hot Cracking Via Magneto-fluid Dynamic Modification of the Laser-Induced Marangoni Convection. In: Sammy Tin, Mark Hardy, Justin Clews, Jonathan Cormier, Qiang Feng, John Marcin et al. (Hg.): Superalloys 2020. Cham: Springer International Publishing (The Minerals, Metals & Materials Series), S. 972–981.

[23] Maiwald, Tim (2017); Defektfreie und endkonturnahe Verarbeitung der Nickel-Basis-Superlegierung CM 247 LC mittels induktionsgestütztem Laser-Pulver-Auftragschweißen; Technische Universität Dresden

[24] Willner, Robin (2015); Konzeptionierung und Aufbau eines kamerabasierten Regelungssystems zur Qualifizierung des dreidimensionalen Laser-Generierens, Technische Universität Dresden

[25] Brueckner, Frank; Finaske, Thomas; Willner, Robin; Seidel, André; Nowotny, Steffen; Leyens, Christoph; Beyer, Eckhard (2015): Laser Additive Manufacturing with Crack-sensitive Materials. In: *LTJ* 12 (2), S. 28–30. DOI: 10.1002/latj.201500015.